J Mater Sci: Mater Med (2017)28:161
DOI 10.1007/s10856-017-5976-6

BIOMATERIALS SYNTHESIS AND CHARACTERIZATION

Original Research

Role of phase separation on the biological performance of 45S5 Bioglass®

Tia J. Kowal[1] · Roman Golovchak[2,3] · Tanuj Chokshi[1] · Joseph Harms[3,4] · Ukrit Thamma[2] · Himanshu Jain[2] · Matthias M. Falk[1]

Received: 22 March 2017 / Accepted: 1 September 2017

Abstract We analyzed the biological performance of spinodally and droplet-type phase-separated 45S5 Bioglass® generated by quenching the melt from different equilibrium temperatures. MC3T3-E1 pre-osteoblast cells attached more efficiently to 45S5 Bioglass® with spinodal than to the one with droplet morphology, providing the first demonstration of the role of micro-/nano-scale on the bioactivity of Bioglass®. Upon exposure to biological solutions, phosphate buffered saline (PBS) and cell culture medium (α-MEM), a layer of hydroxyapatite (HA) formed on both glass morphologies. Although both Bioglass® varieties were incubated under identical conditions, and physico-chemical characteristics of the HA layers were similar, the adsorption magnitude of a model protein, bovine serum albumin (BSA, an abundant blood serum component) and its β-sheet/β-turn ratio and α-helix content were significantly higher on spinodal than droplet type Bioglass®. These results indicate that: (i) a protein layer quickly adsorbs on the surface of 45S5 Bioglass® varieties (with or without HA layer), (ii) the amount and the conformation of adsorbed proteins are guided by the glass micro-/nano-structure, and (iii) cell attachment and proliferation are influenced by the concentration and the conformation of attached proteins with a significantly better cell adhesion to spinodal type 45S5 Bioglass® substrate. Taken together, our results indicate that the biological performance of 45S5 Bioglass® can be improved further with a relatively simple, inexpensive fabrication procedure that provides a superior glass micro-/nano-structure.

Graphical abstract A simple modification to the fabrication procedure of classic 45S5 Bioglass® generates spinodal (A(a)) and droplet (A(b)) varieties and has a significant impact on protein adsorption (B) and cell adhesion (C).

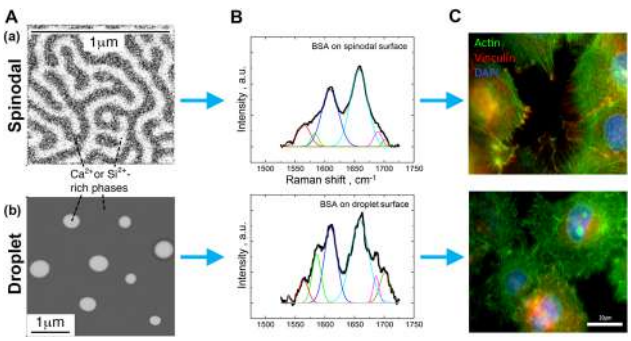

Electronic supplementary material The online version of this article (https://doi.org/10.1007/s10856-017-5976-6) contains supplementary material, which is available to authorized users.

Tia J. Kowal and Roman Golovchak contributed equally to this work.

Himanshu Jain and Matthias M. Falk jointly supervised to this work.

✉ Himanshu Jain
H.Jain@Lehigh.edu

✉ Matthias M. Falk
MFalk@Lehigh.edu

[1] Department of Biological Sciences, Lehigh University, Bethlehem, PA 18015, USA

[2] Department of Materials Science and Engineering, Lehigh University, Bethlehem, PA 18015, USA

[3] Department of Physics and Astronomy, Austin Peay State University, Clarksville, TN 37044, USA

[4] Present address: Nuclear and Radiological Engineering and Medical Physics Programs, The George W. Woodruff School of Mechanical Engineering, Georgia Institute of Technology, Atlanta, GA 30332, USA

Published online: 13 September 2017

1 Introduction

A bioactive glass with the composition 24.4 mol% Na_2O–26.9 mol%CaO–2.6 mol%P_2O_5–46.1 mol%SiO_2, and called 45S5 Bioglass®, was first developed by Larry Hench in the 1960's [1]. He discovered that when placed into simulated body fluid (SBF), the 45S5 Bioglass® formed a robust hydroxyapatite ($Ca_5(PO_4)_3OH$) layer on its surface, which is the main inorganic component of bone [2–4]. Analysis of 45S5 Bioglass® implanted into femurs and tibias of rats, canines and monkeys showed that bone cells efficiently bonded to the glass and accepted it as a bioactive material [1, 5]. Since then, many variations of bioactive glasses have been produced, all with the purpose of engineering improved materials for tissue regeneration [1–3, 6–10]. Some bioactive glasses were, for example, designed with a specific dissolution rate, with macro-pores to allow for cells to migrate into the material, or with anti-microbial properties [6, 7, 10, 11]. Along this line, we have reported on improved bioactive glass scaffolds with TAMP (Tailored Amorphous Multi Porous) structure, which contain both interconnected nano- and macropores [11–15].

The importance of nanotopography on the ability of cells to attach to biomaterials is now well established [16, 17], and also has been demonstrated for bioactive glasses [12]. Remarkably, these studies showed that cells are able to 'sense' the nanostructure of the substrate at a scale that is approximately 1000 times smaller than the cells themselves and in the size-range of individual integrin cell-adhesion receptors (11–19 nm depending on the state of activity) [18–20]. Later, it was reported that even traditional 45S5 Bioglass® can be prepared with different morphologies related to phase separation, as determined by the melt quenching during glass fabrication procedure [21]. However, influence of the type of phase separation on the bioactivity of these materials has not been investigated. Here we report on the influence of phase separated microstructure of these differently melt-quenched 45S5 Bioglass® varieties on their ability to adsorb proteins and adhere cells, in a first attempt toward establishing the role of different morphologies of Bioglass® at the micro- and nanometer scale on cell response. To understand the difference in the response of cells, we have focused on the growth of hydroxyapatide (HA) layer and adsorption of proteins, since these processes influence the surface that is exposed to cells during attachment. In the past, the HA layer has been credited for the superior bioactive properties of 45S5 Bioglass® [22], however there is little published information about what role, if any, adsorbed proteins abundantly present in biological solutions may play toward cell attachment. Since adhered cells remain in contact with culture medium, potential changes in its chemistry have been monitored as well.

2 Materials and methods

2.1 Glass fabrication

45S5 Bioglass® ($45SiO_2$—$24.5Na_2O$—24.5CaO—$6P_2O_5$ by wt. %) was synthesized using melt quenching and casting in stainless steel molds. High purity (99.99 % or better; Alfa Aesar, MA, USA) carbonates ($CaCO_3$, Na_2CO_3), silicon dioxide (SiO_2) and calcium phosphate tribasic ($Ca_5OH(PO_4)_3$) powders (Alfa Aesar, MA, USA) were used as raw precursors, and melted in a platinum crucible. To induce spinodal phase decomposition, the melt was quenched from ≥ 1380 °C into preheated molds (termed "spinodal" glass). Quenching from ≤ 1370 °C produced 45S5 Bioglass® with pronounced droplet type phase separation (termed "droplet" glass) [21]. Post-cooling, cylindrical casts were cut into approximately 2 mm thin disks using a low-speed diamond-plate circular saw (Iso-Met, Buehler, IL, USA), polished to optical quality using a series of silicon carbide abrasive papers with decreasing particle size (d) (paper #120 with $d = 125$ µm; #240 with $d = 58$ µm; #800 with $d = 8$ µm; #1200 with $d = 3$ µm) and finally with 1 µm size CeO_2 powder on an automatic polishing machine (ATA, Sapphir500, Germany). Polished glass samples were cleaned in acetone prior to use.

2.2 X-ray photoelectron spectroscopy of uncoated and protein-coated glass samples

Polished and acetone-cleaned glass samples were rinsed with deionized (DI) water, dried, and characterized initially with high-resolution X-ray photoelectron spectroscopy (XPS). Then the samples were submerged into an aqueous bovine serum albumin (BSA) protein solution (2.5 mg/ml) for 2 h at room temperature. Additionally, a set of samples was sterilized by autoclaving and incubated in 1xPBS (phosphate buffered saline) at 37 °C for 3 days prior to incubation in BSA/PBS (2.5 mg/ml) solution for 2 h. All samples after immersion were washed with DI water to remove excess salts/protein and dried before XPS analyses. The high-resolution XPS measurements were performed with a Scienta ESCA-300 spectrometer using monochromatic Al K_α X-rays (1486.6 eV). XPS spectra were recorded in a normal emission mode, using a low energy (<10 eV) electron flood gun to neutralize surface charging from photoelectron emission. The XPS data consisted of survey scans over the entire binding energy (BE) range and selected scans over the core-level photoelectron peaks of interest. Data were collected from different locations of the same samples (at least 5/sample) as well as on different samples (n = 3/sample type) to confirm the reproducibility of results. This resulted in compositional data, calculated as a ratio between the areas of core level XPS peaks of

constituent chemical elements and appropriate sensitivity factors, with maximum statistical uncertainty of ±2%.

2.3 Raman spectroscopy of protein-coated glass samples

To characterize the structure of proteins adsorbed to glass surfaces, Raman spectroscopy measurements were performed in the 800–2000 cm^{-1} range with a Horiba Xplora confocal microscope (Horiba, NJ, USA), using a 532 nm laser for excitation. Spectra collected from five different locations of each sample were averaged to increase confidence in the data. Peaks for BSA were assigned to known structural motifs (α-helix, β-sheet, and β-turn) according to published literature. To calculate β-sheet/β-turn ratio, the β-sheet band area was divided by the average area of the two assigned β-turn bands as per Gaussian fit with all parameters freed.

2.4 SEM and ESEM surface analyses of uncoated and protein-coated glass samples

Scanning electron microscopy (SEM) images of the microstructure of the prepared glasses were acquired from freshly fractured surface of the glass samples using a Hitachi 4300 (USA) SEM in high-vacuum mode at 12,000x and 18,000x magnification. To examine the Bioglass® samples with adsorbed protein coat under physiological (wet) conditions, polished specimens were imaged as reference before protein-incubation with a FEI XL-30 environmental scanning electron microscope (ESEM) at 250×, 500×, 1000×, and 5000× magnification using the gaseous secondary electron detector (GSE) at approximately 30% humidity. Then, samples were submerged in bovine serum albumin (BSA) (2.5 mg/ml)/DI water protein solution for 2 h at room temperature and re-imaged immediately (wet) under the same conditions. After drying of the samples, a third set of images was acquired (dry).

Additionally, to examine formation of hydroxyapatite (HA) and/or other alterations of the glass surface that may occur upon exposure to medium containing phosphate ions, images were collected using a Zeiss 1550 electron microscope. As described above, samples were pre-incubated in PBS before exposure to BSA solution, then dried overnight in a desiccator before imaging at 1000×, 6000×, and 18,000× magnification.

2.5 pH, colorimetric calcium, and phosphate concentration measurements

Samples were autoclaved for sterilization followed by incubation in 1× PBS at 37 °C. After 3 days, PBS was replaced with cell culture medium (described below) and incubated for 2 and 24 hrs. The medium was collected and pH measured immediately to prevent any potential changes due to environmental exposure. Calcium (Ca^{2+}) and phosphate ion (PO_4^{3-}) concentrations were measured in PBS solution and cell culture medium using Quantichrom bio kits (BioAssays Systems, Hayward, CA; Cat. # DICA-500 and DIPI-500, respectively). To measure calcium in solution a standard curve using the supplied reference solutions was generated. Five microliter of medium was incubated with 200 µl of working reagent. Reactions continued for 3 min at room temperature before absorbance was measured at 612 nm using a Tecan Infinite M200 PRO spectrophotometer. Each solution was measured in triplicate. To measure phosphate in solution, the Quantichrom Phosphate assay and a standard curve prepared using the supplied solutions was implemented. 50 µl of each sample were diluted 1:50 with DI water and incubated in a 96-well plate together with 100 µl of working reagent at room temperature for 30 min. Absorbance was measured for each solution in triplicate at 620 nm.

2.6 Cells and cell assays

MC3T3-E1 subclone 4 mouse pre-osteoblast cells (CRL-2593) were purchased from American Type Culture Collection (ATCC, Manassas, VA). Cells were maintained at standard culture conditions at 37 °C in a 5% CO_2 atmosphere and 100% humidity in complete culture medium as follows: Alpha-Modified Eagles Medium (α-MEM, Gibco/Invitrogen, Grand Island, NY, cat. # A10490-01) was supplemented with 10 % fetal bovine serum (Atlanta Biologicals, Flowery Branch, GA, Cat. # S11150), 1% L-glutamine (HyClone, Logan, UT, Cat. # 25-005-C1) and 1% penicillin/streptomycin (Corning, Corning, NY, Cat. # 30-001-Cl) according to vendor's instructions.

Before cell seeding, polished and acetone-cleaned glass samples were sterilized by autoclaving and pre-incubated in 1xPBS for 3 days at 37 °C. MC3T3-E1 cells were seeded at a density of 35,000 cells/cm^2 onto respective glass disks placed into 3.5 cm diameter polystyrene tissue culture dishes (Corning, Corning, NY, Cat. # 353001). Cells were processed for analysis by fluorescence detection of nuclei by incubating in DAPI solution (Molecular Probes, Eugene, OR, Cat. # D1306), actin by incubating in Alexa488-phalloidin solution (Molecular Probes, Cat. # A-12379), and focal adhesions by immunofluorescence detection of the protein vinculin. In brief, cells were fixed using 3.7% formaldehyde followed by permeabilization with 0.2 % Triton X-100. Then, cells were blocked in 1 % BSA/1 × PBS at room temperature for 1 h. The primary antibody, anti-vinculin (mouse monoclonal-Sigma, St. Louis, MO—Cat. #V9131; at 1:200), was diluted in blocking solution and incubated with cells overnight at 4 °C. A solution of 1xPBS containing DAPI (1 µg/ml:), Alexa488-phalloidin

(1:100), and secondary antibody, Alexa568-conjugated goat-anti-mouse (1:200) (Molecular Probes/Invitrogen, Grand Island, NY, Cat. # A11031) was incubated with the cells at room temperature for 1 h. Samples were placed with cells facing down in 1 x PBS into glass-bottom culture dishes (LabTek) for microscopic examination. Cells were imaged using a Nikon Eclipse TE2000-E inverted fluorescence microscope equipped with 10×, 40×, 60× and 100× objectives and a forced-air cooled Photometrics CoolSnap HQ CCD camera (Roper Scientific, Martinsried, Germany). Images were captured using MetaVue (Molecular Devices, Sunnyvale, CA) software version 6.1r5.

To quantify the number of cells attached to each sample, cell nuclei were counted for each of 6 images acquired with a 10× objective (approximate imaging field = 1 mm^2) for each sample (2 h time point, n = 5; 24 h time point, n = 4). Statistical analyses were performed by ANOVA followed by a *Bonferroni* correction to reduce the chance of obtaining a false positive, which reduced the p-value from p = 0.05 to p = 0.0167, increasing the stringency of the statistical analyses. Average cell size was determined on images of Alexa488-phalloidin stained cells (i.e. actin) by outlining the periphery of individual cells and measuring the cell area using ImageJ software (droplet samples, n = 44; spinodal samples, n = 23 cells). Abundance of peripheral actin (stress fibers) was analyzed by drawing 7.5 × 7.5 μm squares (=55 μm^2) near the periphery of Alexa488-phalloidin stained cells. Fluorescence intensity within the square areas was measured using ImageJ (droplet-type samples, n = 40; spinodal samples, n = 27). Similarly, abundance and robustness of focal adhesions was analyzed by drawing 10 × 10 μm squares (=100 μm^2) near the periphery of vinculin stained cells and measuring fluorescence intensity within the squares (droplet-type samples, n = 15; spinodal samples, n = 12).

3 Results

3.1 Bioglass® morphologies

By casting traditional 45S5 Bioglass® from different equilibration temperatures (≥1380 °C compared to ≤1370 °C), we produced Bioglass® samples with two types of phase separated morphologies: (i) spinodal type when the melt was quenched from temperature ≥ 1380 °C (Fig. 1a),

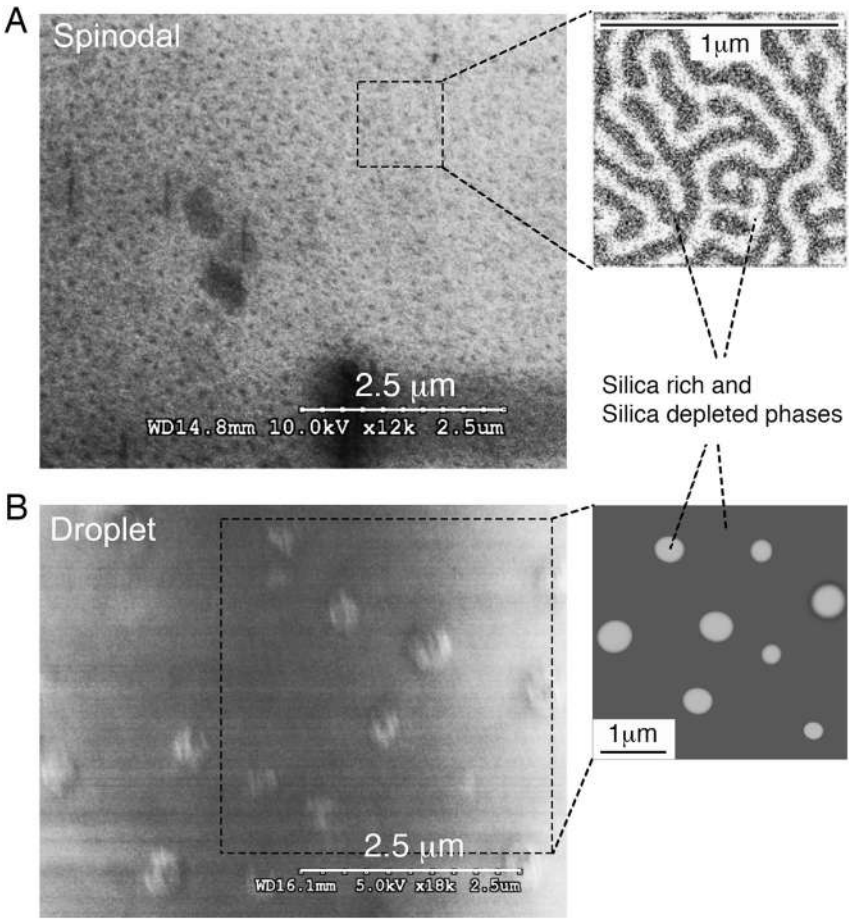

Fig. 1 45S5 Bioglass® varieties with different morphologies. 45S5 Bioglass® samples with spinodal and droplet type phase-separation morphologies were prepared by quenching the melt from different equilibration temperatures following specific regimens. Representative SEM images of the two varieties are shown in **a** and **b**. Simplified schematics of the morphologies to the right illustrate that silicon enriched and depleted regions co-exist in the two 45S5 Bioglass® varieties

Table 1 Composition of as-polished spinodal and droplet type phase-separated 45S5 Bioglass® samples before and after exposure to 0.25% (w/v) aqueous BSA-protein solution as determined by XPS surface analyses

Sample	Composition in at%					
	O	Si	Ca	Na	P	N
Glass composition, theoretical	55.2	16.3	9.5	17.2	1.8	0
Spinodal, as polished	56.9 ± 1.2	13.9 ± 1.7	6.8 ± 1.5	20.6 ± 1.8	1.8 ± 1.0	0
Spinodal, exposed to PBS solution	61.2 ± 2.0	<1	20.9 ± 2.0	<1	16.3 ± 1.5	0
Spinodal, exposed to BSA solution	54.5 ± 1.7	14.5 ± 2.0	4.6 ± 1.7	4.3 ± 1.9	1.6 ± 1.3	20.5 ± 1.5
Spinodal, exposed to PBS then BSA solution	57.0 ± 2.0	<1	10.8 ± 2.0	<1	9.1 ± 1.5	22.0 ± 0.5
Droplet, as polished	57.0 ± 1.2	18.6 ± 1.9	6.9 ± 1.5	15.5 ± 1.8	1.9 ± 1.1	0
Droplet, exposed to PBS solution	60.6 ± 2.0	<1	22.2 ± 2.0	<1	15.8 ± 1.4	0
Droplet, exposed to BSA solution	56.3 ± 1.8	18.4 ± 2.0	4.3 ± 1.8	6.5 ± 2.0	1.7 ± 1.5	13.4 ± 1.6
Droplet, exposed to PBS then BSA solution	55.9 ± 2.0	<1	15.8 ± 2.0	<1	12.5 ± 1.5	14.7 ± 0.5
Hydroxyapatite (HA)	60.8		21.7		13.0	

and (ii) droplet type when quenched from temperatures <1380 °C (Fig. 1b) [21]. The scale of droplet type phase separation in the glass is on a submicron scale, whereas the scale of spinodal phase separation was found to be much smaller (Fig. 1) [21].

In order to evaluate their chemical characteristics, the surfaces of the two Bioglass® varieties were analyzed by XPS in their pristine and polished states. Analyses described earlier [21] demonstrated that the overall chemical composition of both pristine glass varieties were nearly identical. In addition, their compositions were very similar to the calculated theoretical composition (Table 1). Both findings confirm their chemical identity as 45S5 Bioglass®. After polishing, a slight difference in the surface concentration of sodium and silicon was detected between the two sample types (Si: 13.9 ± 1.7% in spinodal, and 18.6 ± 1.9% in droplet; Na: 20.6 ± 1.8% in spinodal, and 15.5 ± 1.8% in droplet, Table 1). This difference may be due to Na^+ leaching out more efficiently from the droplet than the spinodal-type phase separated glass samples; or a more pronounced Na^+ ion migration during polishing towards the surface in spinodal samples [23]. However, these changes were observed in a thin surface layer after polishing only. The underneath bulk composition was found to be comparable for both droplet and spinodal-type phase separated glass samples, and close to the theoretical value of 45S5 Bioglass® [21].

3.2 Attachment and morphology of cells seeded on Bioglass® varieties

MC3T3-E1 pre-osteoblast cells, frequently used in studies investigating the osteo-inductive properties of bioactive glasses [24, 25], were seeded onto the surface of spinodal and droplet type Bioglass® samples. Attached cells were fixed after 2 and 24 h and processed for the detection of cell nuclei using fluorescent chromatin (DAPI, blue) staining (Fig. 2a). Cell nuclei were counted to determine the number of cells that had attached to the surface of the glasses. After merely 2 h, based on the number of attached cells a clear preference of the cells for the glass samples with spinodal morphology compared to the droplet morphology (n = 5) was observed. On average more than double the number of cells (spinodal: 203 ± 4.4 cells vs. droplet: 80.8 ± 6.5 cells) attached to the surface of spinodal phase-separated glass samples compared to droplet type phase-separated glass samples (Fig. 2b). A similar result was observed after 24 h (spinodal: 213 ± 13.2 cells vs. droplet: 84 ± 7.5 cells, n = 4), with more than 2 times the number of cells attached to the spinodal glass than the droplet glass (Fig. 2a, b). Together, these results indicate that MC3T3-E1 cells attached more efficiently to spinodal than to droplet type phase-separated Bioglass® samples.

To determine whether the preference of cells for spinodal glass was also supported by morphological features that typically are associated with cell attachment, we stained the actin cytoskeleton and focal adhesions in cells on both glass varieties after 2 h of exposure. Cellular actin organization was detected by decorating actin with Alexa488-labelled phalloidin (green). The presence, number and robustness of assembled focal adhesions were assessed by fluorescence labeling using an antibody targeting vinculin (red), a protein localizing to focal cell adhesion complexes. We observed that cells growing on the spinodally phase separated Bioglass® samples assembled robust actin stress fibers that preferentially ended in pronounced focal adhesions as is typical of cells growing on stiff substrates. By comparison, cells growing on droplet type phase-separated glass samples assembled an array of much thinner, disoriented actin fibers and only a few, not well-developed vinculin-based focal

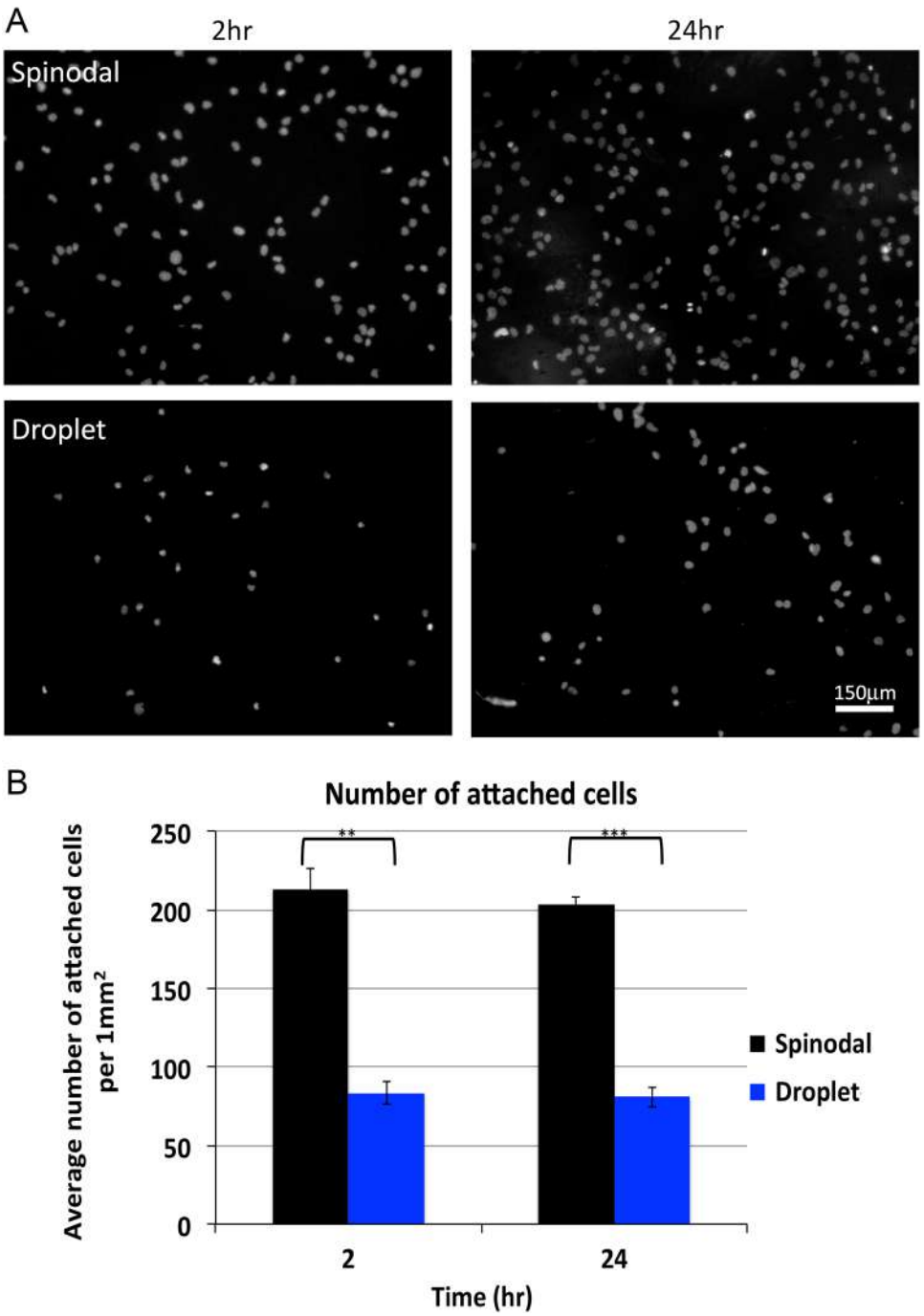

Fig. 2 MC3T3-E1 preosteoblast cells attach more efficiently to spinodally phase separated Bioglass®. **a** Equal numbers of MC3T3-E1 pre-osteoblast cells were seeded onto polished, spinodal and droplet-type Bioglass® varieties. Cells were fixed 2 and 24 h post seeding and cell nuclei stained with DAPI. Representative images are shown. **b** Quantitative analyses based on counting nuclei of five samples and of five areas for each glass type revealed that on average more than two times the number of cells attached to Bioglass® samples with spinodal compared to droplet type morphology

adhesions (Fig. 3a, images in column 1). This significant difference in morphological organization was further exemplified when monochromatic images representing the actin and vinculin channels were black/white inverted and thresholded to enhance the appearance of stress fibers and of focal adhesion complexes (Fig. 3a, images in columns 2 and 3).

To quantify actin and vinculin signal strength, fluorescence intensity of both was measured inside defined squares that were placed in comparable peripheral cytoplasma regions of cells (green and red example squares shown in Fig. 3a). Quantitative analyses (Fig. 3b) showed that cells growing on spinodal glass, on average assembled 65% more stress fibers than cells growing on the droplet glass as indicated by increased peripheral actin fluorescence intensity (Fig. 3b, top right). In addition, we detected 38% more focal adhesion-localized vinculin in cells growing on spinodal samples, indicating that cells growing on spinodal type glass attached more readily to their substrate (Fig. 3b, bottom). Lastly, we observed that the cells growing on

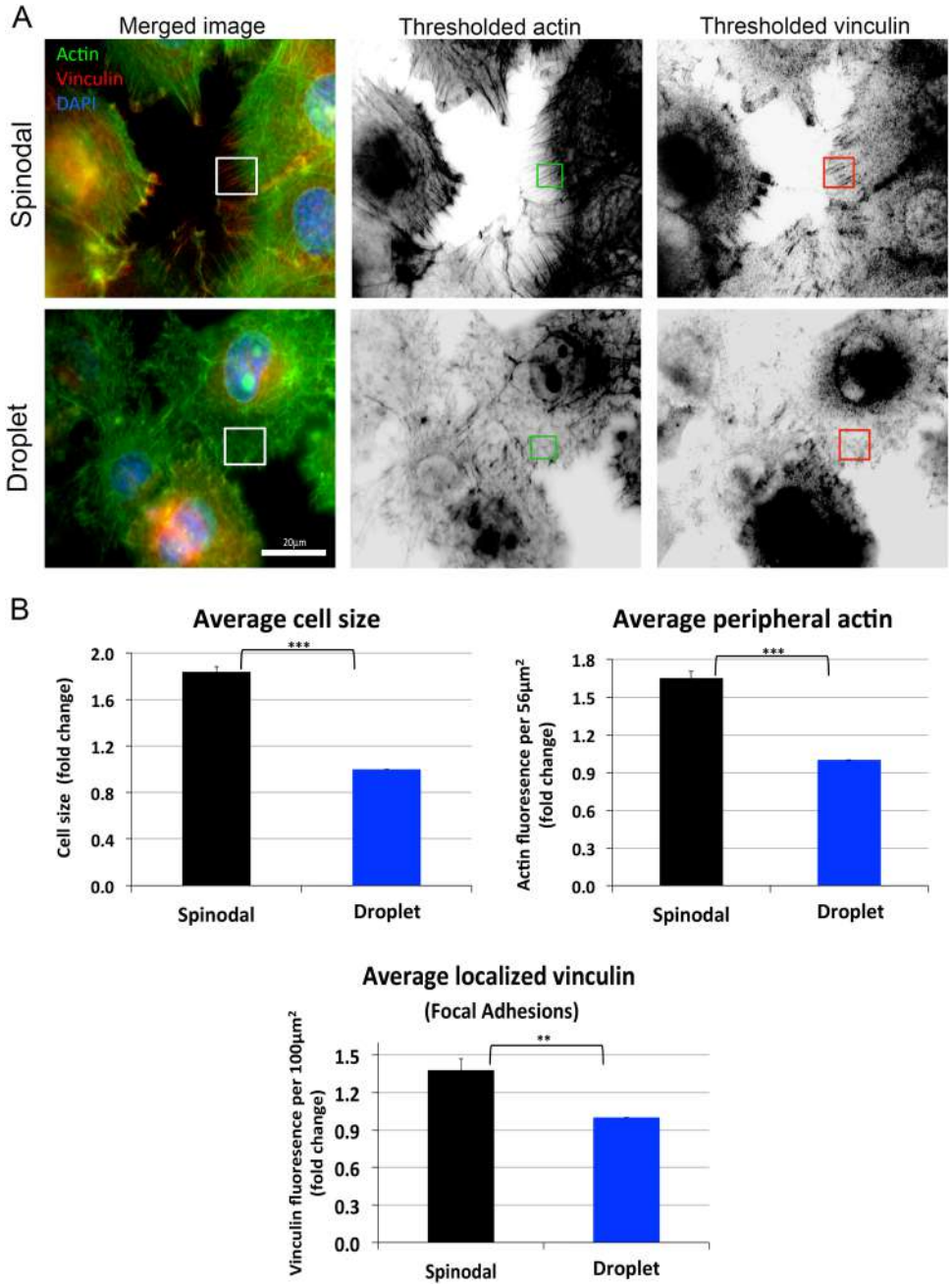

Fig. 3 MC3T3-E1 preosteoblast cells attach more robustly to spinodally phase separated Bioglass®. **a** MC3T3-E1 pre-osteoblasts were seeded onto spinodal and droplet-type Bioglass® samples, fixed and stained 2 h post seeding for actin (phalloidin, green), integrin-based focal adhesions (vinculin, red) and cell nuclei (DAPI, blue). Representative merged images are shown. Monochrome images of actin and vinculin fluorescence channels were black/white converted and thresholded for quantitative analyses. **b** Fluorescence intensities inside defined squares placed in cytoplasmic, plasma membrane-adjacent regions (example squares are shown in **a**) were quantified, averaged and graphed. Note that cells on spinodal-type samples assemble robust, well-organized stress fibers that often end in pronounced integrin-based focal adhesions. In contrast, cells growing on droplet-type samples assembled much less pronounced, less organized actin filaments and only a few, not well-developed focal adhesions (color figure online)

spinodal type samples on average occupied approximately 84% more surface/cell area compared to cells that attached to droplet type glass (Fig. 3b, top left), indicating that they spread out much faster. Together, these data demonstrate that the cells were able to recognize, differentiate and react to the underlying glass surface.

3.3 Chemical behavior of Bioglass® varieties exposed to biological solutions

To better understand cell behavior in respect to Bioglass® substrate we next investigated Bioglass® performance upon exposure to biological solutions. As ions dissolving from Bioglass® may influence the formation of HA by increasing the local concentration of calcium and phosphate ions in solution [2, 26], or by changing the pH of the solution [27–29], and this may influence cellular activity [27, 28], we analyzed the concentration of calcium (Ca^{2+}) and phosphate (PO_4^{-3}) ions and the pH in the solutions before and after exposure to the differently phase separated Bioglass® samples. We chose to use PBS (phosphate buffered saline) and cell culture medium for these analyses, as both are physiological solutions that are used routinely when culturing cells as opposed to simulated body fluid (SBF)

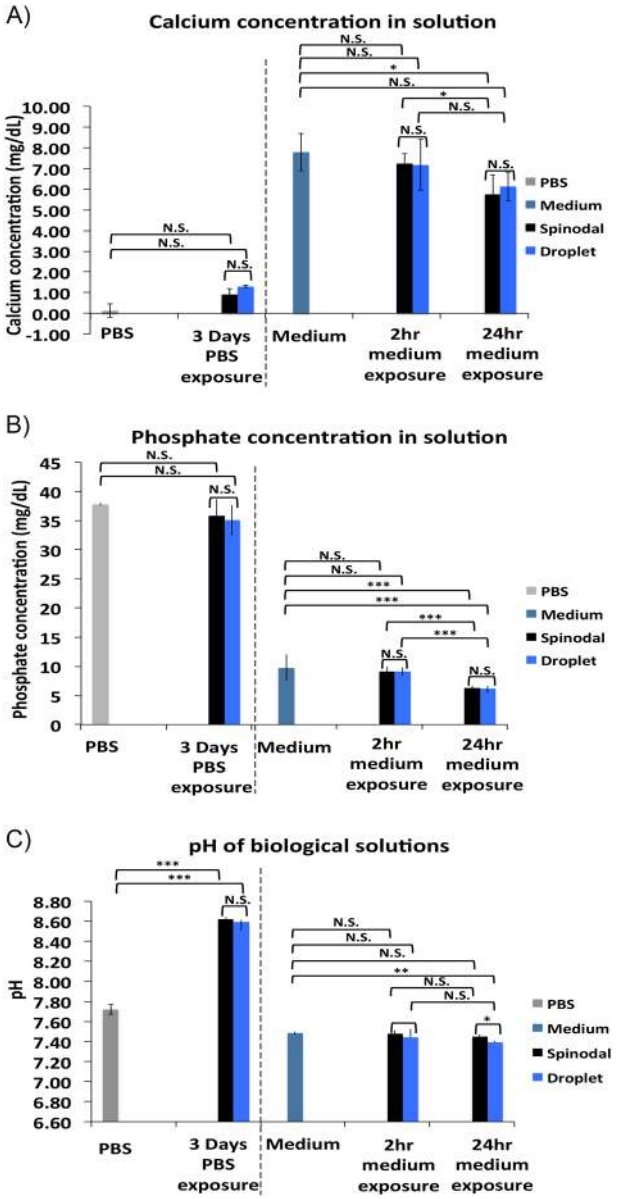

Fig. 4 Effects exposing spinodal and droplet phase-separated Bioglass® samples to biological solutions: calcium, phosphate, and pH. The concentration of Ca (**a**) and P_i (**b**) and the pH (**c**) was measured in phosphate buffered saline (PBS) and cell culture medium before and after exposure to either spinodal or droplet-type phase separated bioactive glass. Ca, P_i, and pH decreased slightly overtime, however no significant differences were detected between the two Bioglass® varieties

which is not appropriately formulated for the culture of mammalian cells [29].

As expected, since PBS does not contain Ca^{2+} ions, no calcium was detected in PBS solution before exposure to glass samples, and only a small amount of Ca^{2+} was detected in the PBS solution after incubation with either glass type (Fig. 4a), suggesting some leaching and/or dissolution of the samples. However, no significant difference in Ca^{2+} concentration was observed between spinodal and droplet type glasses (0.90 ± 0.27 and 1.30 ± 0.07 mg/dL respectively, $n = 4$). In contrast, the concentration of Ca^{2+} in cell culture medium decreased somewhat over time with exposure to both glass types (from 7.78 ± 0.90 mg/dL for medium without glass exposure to 5.75 ± 0.94 mg/dL for spinodal glass and 6.13 ± 0.64 mg/dL for droplet glass after 24 h), suggesting deposition of Ca^{2+} on the glass surfaces eventually leading to HA formation. However, again no significant difference for Ca^{2+} was found for the two Bioglass® varieties (2 h spinodal/droplet: $7.25 \pm 0.47/7.19 \pm 1.24$; 24 h spinodal/droplet: $5.75 \pm 0.94/6.13 \pm 0.69$; Fig. 4a).

A similar result was obtained for PO_4^{3-} (Fig. 4b), with an overall decrease of PO_4^{3-} in solution over time, but no significant difference in the concentration of PO_4^{3-} between spinodal and droplet samples at any time point. The concentration of PO_4^{3-} in PBS solution decreased from 37.8 ± 0.2 mg/dL ($n = 4$) before glass exposure to 35.8 ± 2.8 mg/dL for spinodal glass and 35.0 ± 2.6 mg/dL for droplet glass. Additionally, the concentration of PO_4^{3-} in culture medium decreased from 9.7 ± 2.3 mg/dL (before exposure) to 9.1 ± 0.8 and 9.1 ± 0.7 mg/dL after 2 h and 6.3 ± 0.6 and 6.2 ± 0.8 mg/dL after 24 h for spinodal and droplet glasses, respectively (Fig. 4b), again correlating with the formation of HA on the glass sample surfaces.

A comparable result was also obtained when pH of Bioglass®-exposed biological solutions was determined. On average, the pH of PBS solution before exposure to glass was 7.72 ± 0.05 and increased to 8.62 ± 0.02 (spinodal) and 8.59 ± 0.02 (droplet) after a 3-day incubation period. The pH of cell culture medium before exposure to glass was very similar to the pH of PBS (7.48 ± 0.02, $n = 4$) (Fig. 4c), however in contrast to PBS remained almost unchanged during Bioglass® exposure. After 2-h the pH measured 7.48 ± 0.03 for spinodal and 7.44 ± 0.08 for droplet glass exposed medium samples. After 24 h, the pH dropped slightly to 7.45 ± 0.03 for spinodal, and 7.39 ± 0.02 for droplet glass exposed medium samples (Fig. 4c). Together these data indicate that droplet and spinodal type Bioglass® varieties exhibit very similar dissolution characteristics in biological fluids.

3.4 Formation of hydroxyapatite on Bioglass® varieties

Generally, good biological performance of bioactive glasses is attributed to the formation of a layer of hydroxyapatite (HA) on its surface, which is credited with providing the material with bioactivity [22]. As can be inferred from the comparison of the samples' surface composition obtained through XPS analysis and theoretical composition of HA (Table 1), a HA layer had indeed formed after a 3 day incubation period in PBS solution. As indicated by our

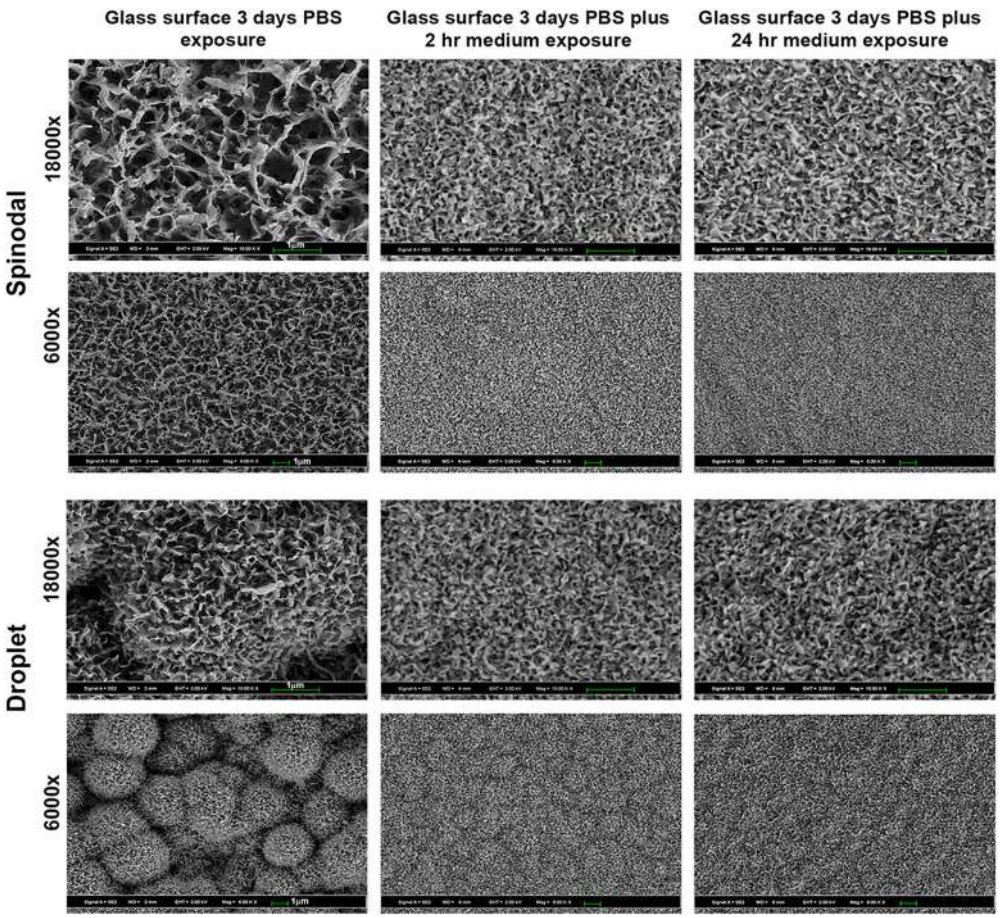

Fig. 5 Surfaces of Bioglass® varieties after incubation in PBS and cell culture medium. Spinodal (top panel) and droplet type (bottom panel) phase-separated Bioglass® samples were investigated by scanning electron microscopy (SEM) after incubation in PBS for 3 days (left columns) and after an additional 2 or 24 h incubation in cell culture medium (middle and right columns respectively). A pronounced HA coat developed on both Bioglass® varieties that appeared more comparable when samples were incubated in PBS followed by cell culture medium as was done in cell culture experiments described in Figs. 1 and 2

measurements summarized in Table 1, there is little observable difference in the concentration of calcium and phosphate on the two Bioglass® varieties, suggesting that the composition of the HA layers was essentially the same. Notwithstanding, to assess the physical structure of the respective HA layers, samples were imaged by SEM after exposure to PBS for 3 days at 37 °C. SEM analyses confirmed the formation of HA layers on both glass varieties (Fig. 5). Both samples were found to be covered with dense, intertwined long lamella- or plate-like HA crystals. However, on the fine structure (18,000× magnification), the HA crystals on the spinodal type Bioglass® appeared larger in size and less densely packed compared to the crystals that formed on the droplet type Bioglass®. In addition, lower magnification analyses (6000× magnification) indicated that on spinodal type Bioglass®, HA deposited as a more or less homogenous smooth layer of lamella-like crystals, whereas on droplet type Bioglass®, HA formed 'boulders' reminiscent of the underlying phase separation. In fact, the center-to-center distance between HA boulders correlated well with the phase-separation features of the droplet type Bioglass® samples (compare Figs. 1 and 5).

Since Bioglass® samples were pre-incubated for 3 days in PBS followed by incubation in medium when cells were seeded on the glass samples, analyses of the structure of the HA coat that formed under these conditions was performed as well. The resulting SEM images convincingly show little variation in the structure of the HA crystals once the glass samples were submerged in cell culture medium after either 2 or 24 h (Fig. 5, middle and right panels). Moreover, pronounced HA 'boulders' that were detected on droplet-type Bioglass® samples after incubation in PBS solution partially disappeared, making the overall morphology of HA coats that formed on both Bioglass® varieties much more similar (Fig. 5, middle and right panels).

3.5 Adsorption of protein to Bioglass® variety surfaces —ESEM and XPS analyses

To investigate whether spinodal and droplet type Bioglass® varieties would absorb a coat of proteins to their surface when exposed to bodily fluids, we incubated the samples in a model protein solution, bovine serum albumin (BSA), that is abundantly present in blood serum as well as in the serum component of cell culture medium [30]. We first applied environmental scanning electron microscopic (ESEM) analyses of wet and dry Bioglass® samples that were incubated in BSA-solution or not. All samples appeared similarly un-contoured, both at lower [500×] and higher (5000×) magnifications, suggesting that if a protein coat had formed, it must be thin and overall of homogenous appearance (Fig. S1). Note these samples were not pre-incubated in PBS solution; hence no HA coat is present on the samples.

Next, we used XPS to better determine whether a coat of protein had adsorbed to the sample surfaces. A pronounced nitrogen (N) signal was detected by XPS analyses on all samples that were submersed in BSA-solution (Fig. S2) but not on the bulk glass, indicating that indeed a protein coat had formed on the surfaces of the BSA-incubated samples. Moreover, the percentage of nitrogen detected in the BSA-coated spinodal type Bioglass® samples was significantly higher compared to droplet type samples ($20.5 \pm 1.5\%$, compared to $13.4 \pm 1.6\%$, Table 1), suggesting that more protein adsorbed to spinodal compared to droplet-type Bioglass® samples. Additionally, the amount of Ca and particularly the amount of Na detected by XPS on the glass samples immersed in BSA solution was significantly reduced (Ca on spinodal: $6.8 \pm 1.5\%$ before, $4.6 \pm 1.7\%$ after immersion; Ca on droplet: $6.9 \pm 1.5\%$ before, $4.3 \pm 1.8\%$ after immersion; Na on spinodal: $20.6 \pm 1.8\%$ before, $4.3 \pm 1.9\%$ after immersion; Na on droplet: $15.5 \pm 1.8\%$ before, $6.5 \pm 2.0\%$ after immersion, Table 1), further suggesting that a thin layer of protein had coated the Bioglass® surface.

Additionally, XPS analyses of the surfaces of spinodal and droplet Bioglass® samples after 2 h pre-incubation in PBS (and hence with a layer of HA present on their surface) led to a significant difference in the detection of nitrogen (Table 1), indicating that BSA robustly adsorbed to both, HA and polished Bioglass® sample surfaces; and again, that more protein adsorbed to the HA layer on spinodal type Bioglass® compared to the amount adsorbed to HA-coated droplet-type Bioglass® surfaces (concentration of N ~ 22.0 ± 0.5 vs. $14.7 \pm 0.5\%$, Table 1). Combined, our data indicate that indeed a thin protein film (still allowing detection of the underlying glass and HA chemistry) had formed on both Bioglass® surfaces (too thin for ESEM detection), with significantly more protein adsorbing to spinodal Bioglass® samples.

3.6 Conformation of proteins adsorbed on Bioglass® samples—Raman spectroscopy

To investigate whether BSA adsorbed to spinodal and droplet phase separated Bioglass® varieties adopted different conformations we applied Raman spectroscopic analyses. Both, infrared (IR) and Raman vibrational spectroscopies have been used successfully in the past to analyze the conformational state of proteins such as BSA adsorbed on different glass surfaces [31–35]. The amide groups of proteins possess nine characteristic vibrational modes or group frequencies [35]. Of these, the most useful for vibrational spectroscopic analysis of the secondary structure of proteins in aqueous media is the so-called Amide I band located between ~1600 and 1700 cm^{-1} [31–35]. This band represents primarily the C=O stretching vibrations of the amide groups coupled to the in-plane N-H bending and C-N stretching modes [32, 33, 35]. The exact frequency of this vibration is determined by the particular secondary structure adopted by the polypeptide chains. However, when conformations of proteins in solution are of interest, Raman spectroscopy is usually preferred over IR spectroscopy as the signal at 1645 cm^{-1} from water is very weak in Raman spectra (corresponding vibrations have very low Raman activity) and thus does not interfere with the reliable detection of the critical Amide I band. The Raman Amide I band representing the contours of BSA protein and shown in Fig. 6 consists of a number of overlapping component bands, representing α-helices, β-sheets, β-turns and non-ordered structures comparable to previous analyses [31–35]. The exact assignments of the observed Raman peaks in the Amide I band (shown in Fig. 7a–c) were made on the basis of known data [32, 33, 35], and are summarized in Fig. 7d. Decomposition of the experimental Raman spectra of the Amide I band into Gaussians (Fig. 7d) allows for evaluating the β-sheet/β-turn ratio, which is known to indicate biocompatibility of the material under consideration [31, 34, 35]. We determined a 2–3 times higher β-sheet/β-turn ratio and also an increased α-helix content for BSA-polypeptides adsorbed to spinodally phase separated Bioglass® in comparison to droplet type phase separated glass (Fig. 7d). Interestingly, the α-helix content in BSA-polypeptides adsorbed on both Bioglass® varieties was lower compared to lyophilized BSA, further indicating that the conformation of BSA-polypeptides adsorbed on the Bioglass® samples was modified (less ordered). This observation is in agreement with previous findings on proteins adsorbed to other biomaterials [16, 36].

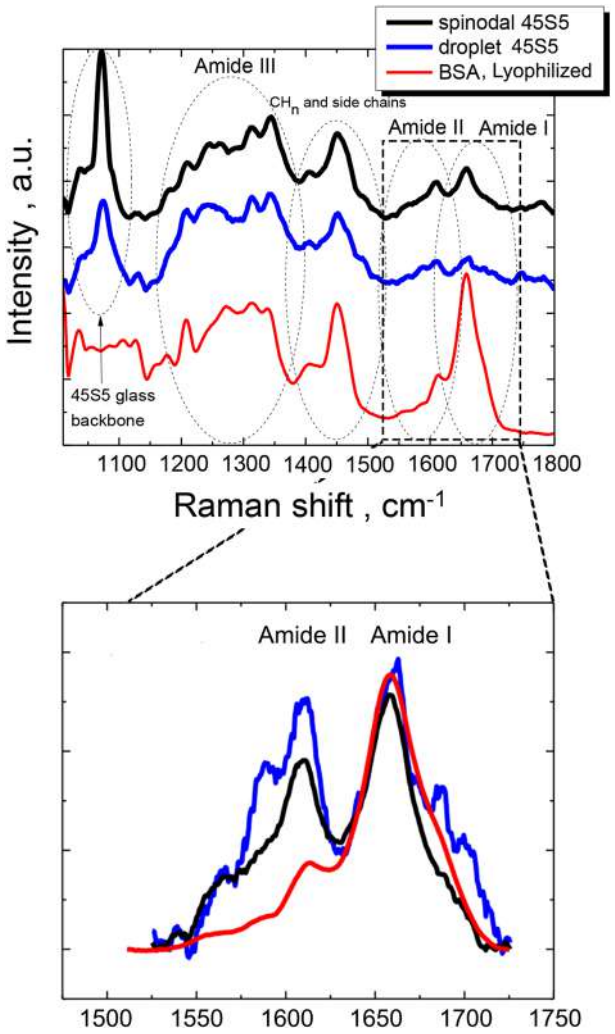

Fig. 6 Raman spectra of protein-coated Bioglass® varieties. Representative Raman spectra of lyophilized bovine serum albumin (BSA, red), and 45S5 Bioglass® varieties after incubation in aqueous BSA solution (spinodal, black; droplet, blue). Note the Amide I and II bands (enlarged and superimposed below) in all samples indicative of a protein layer that adsorbed on the glass sample surfaces (color figure online)

4 Discussion

Conventional 45S5 Bioglass® invented by Hench in the 1960s has mostly been considered to be a structurally homogeneous, single phase glass [1, 10, 37, 38]. However, this may not always be true [39–41], as the morphology of Bioglass can for example be modulated following a simple melt-quench procedure, resulting in spinodal vs. droplet-type phase separation [21]. In the Bioglass® samples investigated here, the two types of phase-separation arise from the difference in the melt temperature just prior to casting and the quench rate during solidification [21]. We show that the type of phase separation can have a pronounced effect on cellular response. Thus, better understanding Bioglass®/cell interaction appears crucial for the future design of improved bioactive glass applications.

When seeding MC3T3-E1 pre-osteoblast cells on the two phase-separated Bioglass® varieties we found that, on average, more than double the number of cells attached to the surface of spinodal glass at 2 and 24 h post seeding as compared to droplet-type phase-separated Bioglass® samples. Increased cell adhesion correlated with significantly increased cell spreading (individual cells on average covered 84% more area on spinodal glass samples), the formation of significantly more, and more robust stress fibers (by 65%), and better-developed focal cell adhesions (by 38%). What then causes the difference in cellular behavior?

As adhered cells are surrounded by culture medium, it is feasible to post that spinodal and droplet Bioglass® varieties differently modify the culture medium (e.g. pH, and the ability to form a HA coat), which in turn would affect cell response. However, when we incubated spinodal and droplet-type phase-separated Bioglass® samples in biological solutions (PBS, cell culture medium), we only observed minimal changes in pH that remained well within the physiological range of biological systems [42, 43]; and both Bioglass® varieties exhibited very similar dissolution characteristics (concentration of Ca^{2+} and PO_4^{3-} in solution over time).

SEM as well as XPS analyses showed that on both Bioglass® varieties a robust layer of HA formed within 3 days in PBS. The chemical composition and the fine structure of the HA crystals was similar on both Bioglass® varieties consisting of comparable dense, intertwined long lamella- or plate-like HA crystals (Fig. 5), yet composed of crystals exhibiting a somewhat different size (Fig. 5, left panels). However, resulting surface roughness differences on this scale are unlikely to produce a discernable difference to the attachment and performance of MC3T3-E1 cells [44]. Interestingly, the morphology of the formed HA layer corresponded to the underlying Bioglass® morphology, with spinodal phase separated samples accumulating an overall homogeneous layer of HA crystals, while droplet-type phase-separated samples accumulated a layer of boulder-like HA clusters. As expected, the boulder center-to-center spacing correlated well with the phase-separated pattern of this Bioglass® variety (compare Figs. 1 and 5). However, when samples were incubated in cell culture medium after exposure to PBS (as was done with Bioglass® samples examined for cell attachment), HA boulders partially disappeared and were much less pronounced, making both HA coats morphologically similar (Fig. 5, middle and right panels), suggesting that differences in HA coat formation also only has a minor impact on cell response.

Intriguingly, XPS analyses further indicted that both Bioglass® varieties absorbed a layer of proteins, either adsorbed directly to the polished glass surface (if samples

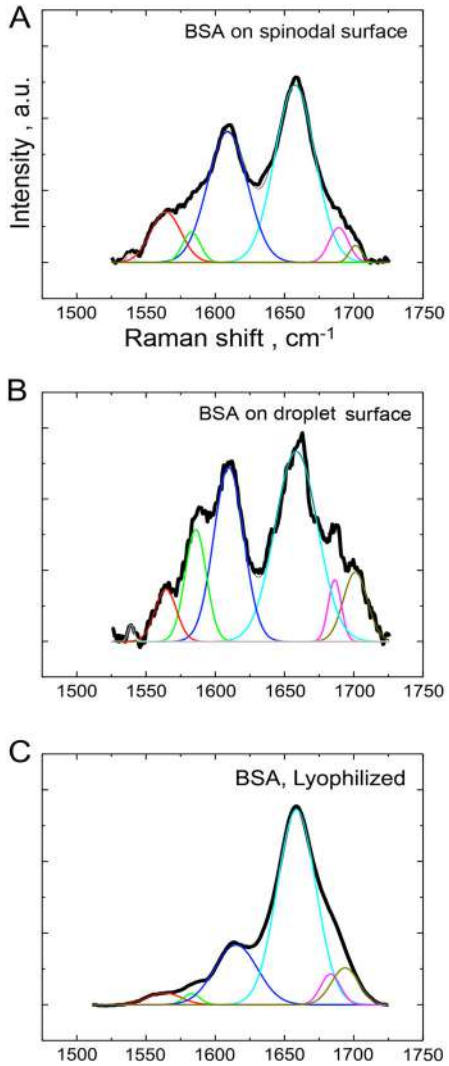

D

Position cm^{-1}	FWHM cm^{-1}	Intensity %	Assignment
BSA adsorbed at 45S5 surface with spinodal phase separation			
1564	25.9	10	Amide II
1583	15.2	4	Amide II
1609	34	34	β-sheet
1658	34.2	47	α-helix
1689	16.4	4	β-turn
1701	10.4	5	β-turn
BSA adsorbed at 45S5 surface with droplet separation			
1564	18.2	6	Amide II
1586	18	12	Amide II
1610	25.5	27	β-sheet
1659	36.3	42	α-helix
1687	11.1	4	β-turn
1701	20.4	9	β-turn
Lyophilized BSA			
1562	28.7	3	Amide II
1583	14.5	2	Amide II
1615	36.4	21	β-sheet
1659	33	61	α-helix
1683	16.7	5	β-turn
1694	23.2	8	β-turn

Fig. 7 Gaussian fittings of Raman spectra indicate a different conformation of BSA adsorbed to spinodal and droplet Bioglass® varieties. Gaussian fittings (colored lines in graphs **a** to **c**) of Raman spectra of dried, BSA-protein coated spinodal (**a**), and droplet type phase separated 45S5 Bioglass® samples (**b**); and **c** of lyophilized BSA. **d** Quantitative analyses of Gaussian fittings of Raman spectra recorded for samples **a** to **c** and assignment of corresponding secondary protein structures according to previously published studies. Note the increased β-sheet and α-helix content of BSA adsorbed to spinodal compared to droplet type phase-separated Bioglass® samples (depicted in red). *FWHM* full width at half maximum of Gaussians

were not incubated in PBS solution or cell culture medium), or on top of the HA layer (see Table 1). As XPS only probes the top ~10 nm of a sample surface, and in all cases the glass or HA chemistry was detectable underneath the protein coat (as indicted by the signal for Si, Ca, and Na, none of which is present in proteins, see Table 1), our results indicate that the protein coat likely is thin, consisting of only 1–2 layers of protein molecules, consistent with reports on protein films that adsorb to the surfaces other biomaterials [16, 17, 45–50]. In its mature, soluble form BSA is a globular protein, which consists of 583 amino acid residues, has a molecular weight of 66.5 kDa, and measures $14 \times 4 \times 4$ nm in diameter [51, 52]. We chose bovine serum albumin (BSA) as a model protein, although it likely is not the protein species that directly interacts with integrin cell adhesion receptors (it has no arginine-lysine-aspartic acid-based amino acid integrin binding sequences, commonly known as RGD signals). However, BSA is abundantly present in blood and the serum component of cell culture medium (61% of all protein present [30]), and thus has the potential to readily adsorb onto the surface of bioactive glasses when exposed to body fluids. Likely, BSA also mediates the adsorption of other, less abundant serum proteins (e.g. ECM proteins) [53], further supporting a critical role of BSA in mediating cellular response to biomaterials surfaces.

Interestingly, we found that significantly more protein adsorbed to spinodal Bioglass® samples compared to droplet-type samples (20.5 ± 1.5%, compared to 13.4 ± 1.6%, Table 1), suggesting that the adsorbed protein potentially formed a thicker, or more homogenously distributed film that may contribute to the better biological performance of the spinodal phase separated Bioglass® samples. Remarkably, Raman spectroscopy further indicated a 2–3 times higher β-sheet/β-turn ratio of BSA-polypeptides adsorbed to spinodally phase separated Bioglass® samples in comparison to BSA polypeptides adsorbed to droplet type phase separated samples. Higher β-sheet/β-turn ratios of adsorbed proteins have been correlated with an increased biocompatibility of protein-coated surfaces [31, 34, 35]. Furthermore, the α-helix content in BSA-polypeptides adsorbed to both Bioglass® varieties was lower compared to the α-helix content of solubilized BSA. As BSA in solution is a well-ordered protein, exhibiting approximately 60% α-helicity [54–56], the observed decrease in α-helicity indicates that BSA polypeptides are less folded when adsorbed to Bioglass®. These observations correlate well with conformational alterations seen generally in proteins that adsorb to other surfaces [16, 36].

As it is now well accepted that proteins in solution (e.g. blood, lymph, or cell culture medium) are readily and robustly adsorbed on the surface of bioactive materials [16, 17, 45–50], we expect that cells did not attach directly to the native Bioglass® surface or to the HA layer, but through a protein film that adsorbed onto the surface of the scaffolds (or the HA layer). The adsorption of proteins on a surface is based on several characteristics of both the material and the protein [16, 17, 47, 49, 50]. Characteristics of the protein include size, charge, and structural stability. For example, larger proteins or structurally unstable proteins that may unfold on contact to a surface are likely to cover a greater surface area on the material compared to smaller, more stable proteins [49, 57]. Additionally, the charge or surface potential, heterogeneity, hydrophilicity/hydrophobicity, composition, and topography of the surface of the material, as well as the pH of the environment can affect how proteins are adsorbed and ultimately affect the material's biological performance [49, 58]. Since HA has been used in protein chromatography for years [59], there is some understanding of how proteins interact with this material. Like the interaction of proteins with other substrates, the main form of interaction is ionic, for example negatively charged carboxyl and phosphate groups of proteins will interact with positively charged calcium of HA [60, 61]. In addition, it has been suggested by Luo and Andrade 1998 [62] that there is cooperativity of adsorption. Cooperativity may be dependent on several factors, including protein conformation. Indeed, one can imagine that as proteins unfold upon adsorption to a substrate (as observed above by the change in α-helical content), their interactions with other proteins may change since new amino acid side chains may be exposed, allowing additional or different proteins to adsorb to the substrate surface.

Whether the glass surface was activated by HA or not apparently did not significantly influence the amount of BSA that adsorbed to the surface of Bioglass®, as the amount of nitrogen detected by XPS analyses was comparable on both, HA-coated and as-polished, uncoated samples. Similarly, Garcia et al. found no difference in the amount of fibronectin (an extracellular matrix protein) that adsorbed to the surface of bioactive glass either unreacted or reacted for 1 day and 7 days in simulated body fluid (SBF) [63]. Furthermore, they found that cells attached more strongly to the glass that had been reacted to form HA and attributed it to the morphology of the adsorbed proteins. In this context, our results suggest that HA formation per se is not required for a glass to be considered bioactive, as proteins present in biological solutions will—upon exposure—likely absorb immediately to the glass surface. However, nanoscale structure of HA, when present, will likely modulate the level of bioactivity by influencing the amount and conformation of proteins that adsorb. We believe that the results described here for BSA will likely extend to other proteins commonly found in cell culture medium, such as fibronectin, since similar results have been reported in literature for the adsorption of other proteins on HA [60–63]. Taken together, our results provide evidence that cell attachment to 45S5 Bioglass® is mediated by a protein layer whose conformational state on spinodally phase-separated glass samples evidently represents a more favorable attachment surface for MC3T3-E1 pre-osteoblast cells. This type of surface makes spinodal Bioglass® varieties biologically favorable over droplet-type phase separated varieties. Apparently, these characteristics are more conducive for cell attachment and proliferation on spinodal than droplet type phase separated Bioglass®.

Although there are potential applications of bulk glasses as prepared here, some bioscaffolds for bone regeneration are prepared by sintering Bioglass® powder. The process of sintering has its own advantages and disadvantages. As a rule, sintering means heating to higher than glass transition (T_g) temperatures, which can result in phase separation and partial crystallization of the Bioglass® leading to the formation of glass-ceramics of complex microstructure. Moreover, phase separation initially present in the parent glass used for sintering has a profound impact on the crystallization of powder particles [21, 64], which, in turn, would have an impact on bioactivity of the scaffold. Therefore, the bioactivity of scaffolds prepared using a sintering method would also depend on nanoscale phase separation of parent glass, which depends on quenching temperature and rate investigated here. Therefore, for

applications using bioactive glass like 45S5 Bioglass® or glass-ceramic as bulk or as sintered powder, its biological performance can be improved further by implementing a relatively simple, inexpensive fabrication procedure that provides a superior nanostructure of the glass.

5 Conclusions

Several important conclusions can be drawn regarding the influence of nano/microstructure of bioactive glass on cell response. The present results demonstrate that firstly a thin film of protein is adsorbed on both spinodal and droplet varieties of 45S5 Bioglass whether or not an HA layer is present. Thus, the cells do not interact with glass directly. Secondly, BSA protein attaches more efficiently on spinodally phase separated 45S5 Bioglass than on droplet type phase separated 45S5 Bioglass of the same composition. Thirdly, MC3T3-E1 pre-osteoblast cells show a significantly stronger preference for attaching to the spinodal morphology compared to the droplet morphology.

Further, the cell-attachment to 45S5 Bioglass is mediated by a protein layer whose amount and conformational state depend on the local chemistry and nanoscale structure of underlying Bioglass/HA surface. These characteristics are more conducive for cell attachment and proliferation on spinodal than droplet type phase separated glass. Evidently, the biological performance of 45S5 bioglass and very likely of other bioactive glass and glass-ceramics can be improved further with a relatively simple, inexpensive fabrication procedure that provides optimized micro-nano structure of glass. Overall, the present results provide new insight into the interactions of proteins and cells with Bioglass scaffolds that should be considered for the future development and use of bioactive glass scaffolds.

Acknowledgements The authors would like to thank Bill Mushock of Lehigh University's microscopy facility for his help with the FEI XL30 ESEM. We thank the National Science Foundation for supporting this work via International Materials Institute for New Functionality in Glass (IMI-NFG, DMR-0844014) and PFI:AIR-TT (IIP-1602057) programs. The work in the laboratory of MMF is supported by the National Institutes of Health (NIH-NIGMS, grant R01 GM55725) and an Innovators' Circle grant from the Abington Health Foundation.

Author contributions TJK performed experiments, evaluated data, wrote sections of the manuscript; generated figures, edited the manuscript; RG performed experiments, evaluated data, wrote sections of the manuscript, generated figures, edited the manuscript; TC performed experiments, evaluated data; JH performed Raman measurements, evaluated data; UT performed analytical experiments; HJ, designed experiments, supervised research, edited manuscript; MMF, designed experiments, supervised research, composed and edited figures and edited the manuscript.

Compliance with ethical standards

Conflict of interest The authors declare that they have no competing interests.

References

1. Hench LL. The story of Bioglass. J Mater Sci Mater Med. 2006;17 (11):967–78.
2. Filgueiras MR, La Torre G, Hench LL, Solution effects on the surface reactions of a bioactive glass. J Biomed Mater Res. 1993;27(4):445–53.
3. Filgueiras MR, LaTorre G, Hench LL, Solution effects on the surface reactions of three bioactive glass compositions. J Biomed Mater Res. 1993;27(12):1485–93.
4. Williams DF. Biocompatibility of orthopedic implants: CRC Press. Lc; 1982.
5. Hench LL, Jones JR, Fenn MB. New materials and technologies for healthcare. Imperial College Press, London; 2012.
6. Baino F, Vitale-Brovarone C. Three-dimensional glass-derived scaffolds for bone tissue engineering: current trends and forecasts for the future. J Biomed Mater Res A. 2011;97(4):514–35.
7. Bellucci D, Cannillo V, Sola A, Chiellini F, Gazzarri M, Migone C. Macroporous Bioglass®-derived scaffolds for bone tissue regeneration. Ceram Int. 2011;37(5):1575–85.
8. Boccaccini AR, Chen Q, Lefebvre L, Gremillard L, Chevalier J. Sintering, crystallisation and biodegradation behaviour of Bioglass-derived glass-ceramics. Faraday Discuss. 2007;136: 27–44 discussion 107–23.
9. Gross U, Kinne R, Schmitz H, Strunz V. Critical reviews in Biocompatibility. Boca Raton, FL: CRC Press; 1988. p. 155.
10. Thomas MV, Puleo DA, Al-Sabbagh M. Bioactive glass three decades on. J Long Term Eff Med Implants. 2005;15(6):585–97.
11. Zhang D, Jain H, Hupa M, Hupa L. In-vitro degradation and bioactivity of tailored amorphous multi porous scaffold structure. J Am Ceram Soc. 2012;95(9):2687–94.
12. Wang S, Kowal TJ, Marei MK, Falk MM, Jain H. Nanoporosity significantly enhances the biological performance of engineered glass tissue scaffolds. Tissue Eng Part A. 2013;19 (13–14):1632–40.
13. Wang S, Falk MM, Rashad A, Saad MM, Marques AC, Almeida RM, et al. Evaluation of 3D nano–macro porous bioactive glass scaffold for hard tissue engineering. J Mater Sci: Mater Med. 2011;22(5):1195–203.
14. Vueva Y, Gama A, Teixeira AV, Almeida RM, Wang S, Falk MM, et al. Monolithic glass scaffolds with dual porosity prepared by polymer-induced phase separation and sol–gel. J Am Ceram Soc. 2010;93(7):1945–9.
15. Marques AC, Almeida RM, Thiema A, Wang S, Falk MM, Jain H. Sol-gel-derived glass scaffold with high pore interconnectivity and enhanced bioactivity. J Mater Res. 2009;24(12):3495–502.
16. Lord MS, Foss M, Besenbacher F. Influence of nanoscale surface topography on protein adsorption and cellular response. Nano Today. 2010;5:66–78.
17. Roach P, Farrar D, Perry CC. Surface tailoring for controlled protein adsorption: effect of topography at the nanometer scale and chemistry. J Am Chem Soc. 2006;128(12):3939–45.
18. Elbe JA. Integrin-ligand interaction. Springer Science & Business Media, Dordrecht; 2013.
19. Nermut MV, Green NM, Eason P, Yamada SS, Yamada KM. Electron microscopy and structural model of human fibronectin receptor. EMBO J. 1988;7(13):4093–9.

20. Ye F, Hu G, Taylor D, Ratnikov B, Bobkov AA, McLean MA. et al. Recreation of the terminal events in physiological integrin activation. J Cell Biol. 2010;188(1):157–73.
21. Golovchak R, Thapar P, Ingram A, Savytskii D, Jain H. Influence of phase separation on the devitrification of 45S5 bioglass. Acta Biomater. 2014;10(11):4878–86.
22. Hench LL. Bioceramics: from concept to clinic. J Am Ceram Soc. 1991;74(7):1487–510.
23. Almeida RM, Hickey R, Jain H, Pantano CG. Low-energy ion scattering spectroscopy of silicate glass surfaces. J Non-Crystalline Solids. 2014;385:124–8.
24. Quarles LD, Yohay DA, Lever LW, Caton R, Wenstrup RJ. Distinct proliferative and differentiated stages of murine MC3T3-E1 cells in culture: an in vitro model of osteoblast development. J Bone Miner Res. 1992;7(6):683–92.
25. Wang D, Christensen K, Chawla K, Xiao G, Krebsbach PH, Franceschi RT. Isolation and characterization of MC3T3-E1 pre-osteoblast subclones with distinct in vitro and in vivo differentiation/mineralization potential. J Bone Miner Res. 1999;14 (6):893–903.
26. Sepulveda P, Jones JR, Hench LL. In vitro dissolution of melt-derived 45S5 and sol-gel derived 58S bioactive glasses. J Biomed Mater Res. 2002;61(2):301–11.
27. Xynos ID, Edgar AJ, Buttery LD, Hench LL, Polak JM. Gene-expression profiling of human osteoblasts following treatment with the ionic products of Bioglass 45S5 dissolution. J Biomed Mater Res. 2001;55(2):151–7.
28. Tsigkou O, Jones JR, Polak JM, Stevens MM. Differentiation of fetal osteoblasts and formation of mineralized bone nodules by 45S5 Bioglass conditioned medium in the absence of osteogenic supplements. Biomaterials. 2009;30(21):3542–50.
29. Bohner M, Lemaitre J. Can bioactivity be tested in vitro with SBF solution?. Biomaterials. 2009;30(12):2175–9.
30. Price PJ, Gregory EA. Relationship between in vitro growth promotion and biophysical and biochemical properties of the serum supplement. In Vitro. 1982;18(6):576–84.
31. Byler DM, Susi H. Examination of the secondary structure of proteins by deconvolved FTIR spectra. Biopolymers. 1986;25 (3):469–87.
32. Gruian C, Vanea E, Simon S, Simon V. FTIR and XPS studies of protein adsorption onto functionalized bioactive glass. Biochim Biophys Acta. 2012;1824(7):873–81.
33. Surewicz WK, Mantsch HH. New insight into protein secondary structure from resolution-enhanced infrared spectra. Biochim Biophys Acta. 1988;952(2):115–30.
34. Tunc S, Maitz MF, Steiner G, Vazquez L, Pham MT, Salzer R. In situ conformational analysis of fibrinogen adsorbed on Si surfaces. Colloids Surf B Biointerfaces. 2005;42(3–4):219–25.
35. Vanea E, Magyari K, Simon V. Protein attachment on aluminosilicates surface studied by XPS and FTIR spectroscopy. J Optoelectron Adv Mater. 2010;12(5):1206–12.
36. Molino PJ, Higgins MJ, Innis PC, Kapsa RM, Wallace GG. Fibronectin and bovine serum albumin adsorption and conformational dynamics on inherently conducting polymers: a QCM-D study. Langmuir. 2012;28(22):8433–45.
37. Renny M, Baltzar S, Mattias E. Na/Ca intermixing around silicate and phosphate groups in bioactive phosphosilicate glasses revealed by heteronuclear solid-state NMR and molecular dynamics simulations. J Phys Chem B. 2015;119(17):5701–15.
38. Renny M, Turdean-Ionescu C, Stevensson B, Izquierdo-Barba I, García A, Arcos D, et al. "Direct probing of the phosphate-ion distribution in bioactive silicate glasses by solid-state NMR: evidence for transitions between random/clustered scenarios. Chem Mater. 2013;25(9):1877–85.
39. Lefebvre L, Chevalier J, Gremillard L, Zenati R, Thollet G, Bernache-Assolant D, et al. Structural transformations of bioactive glass 45S5 with thermal treatments. Acta Mater. 2007;55 (10):3305–13.
40. O'Donnell MD, Watts SJ, Law RV, Hill RG. Effect of P 2 O 5 content in two series of soda lime phosphosilicate glasses on structure and properties–Part I: NMR. J Non-Cryst Solids. 2008;354(30):3554–60.
41. Pedone A, Charpentier T, Malavasi G, Menziani MC. New insights into the atomic structure of 45S5 bioglass by means of solid-state NMR spectroscopy and accurate first-principles simulations. Chem Mater. 2010;22(19):5644–52.
42. Ceccarini C, Eagle H. pH as a determinant of cellular growth and contact inhibition. Proc Natl Acad Sci. 1971;68(1):229–33.
43. Eagle H. The effect of environmental pH on the growth of normal and malignant cells. J Cell Physiol. 1973;82(1):1–8.
44. Jain RH, Wang S, Moawad H, Falk MM, Jain H. Glass bone implants: the effect of surface topology on attachment and proliferation of osteoblast cells on 45S bioactive glass. In: Bhatia S, Bryant S, Burdick JA, Karp JM, Walline K, editors. Engineering biomaterials for regenerative medicine. Mater. Res. Soc. Symp. Proc. Vol. 1235, Warrendale, PA, 2010. 1235-RR03-47.
45. Bahniuk MS, Pirayesh H, Singh HD, Nychka JA, Unsworth LD, Bioactive glass 45S5 powders: effect of synthesis route and resultant surface chemistry and crystallinity on protein adsorption from human plasma. Biointerphases. 2012;7(1–4):41.
46. Effah Kaufmann EAB, Ducheyne P, Radin S, Bonnell DA, Composto R. Initial events at the bioactive glass surface in contact with protein-containing solutions. J Biomed Mater Res A. 2000;52(4):825–30.
47. El-Ghannam A, Ducheyne P, Shapiro IM. Effect of serum proteins on osteoblast adhesion to surface-modified bioactive glass and hydroxyapatite. J Orthop Res. 1999;17(3):340–5.
48. Magyari K, Gruian C, Varga B, Ciceo-Lucacel R, Radu T, Steinhoff HJ, et al. Addressing the optimal silver content in bioactive glass systems in terms of BSA adsorption. J Mater Chem B. 2014;2(35):5799–808.
49. Wang K, Zhou C, Hong Y, Zhang X. A review of protein adsorption on bioceramics. Interface Focus. 2012;2(3):259–77.
50. Wilson CJ, Clegg RE, Leavesley DI, Pearcy MJ. Mediation of biomaterial-cell interactions by adsorbed proteins: a review. Tissue Eng. 2005;11(1–2):1–18.
51. Peters T, editor. The Plasma Proteins. Putman, FW ed: Academic Press, New York; 1975.
52. Wright AK, Thompson MR. Hydrodynamic structure of bovine serum albumin determined by transient electric birefringence. Biophys J. 1975;15(2 Pt 1):137–41.
53. Nilausen K. Role of fatty acids in growth-promoting effect of serum albumin on hamster cells in vitro. J Cell Physiol. 1978;96 (1):1–14.
54. Huang BX, Kim HY, Dass C. Probing three-dimensional structure of bovine serum albumin by chemical cross-linking and mass spectrometry. J Am Soc Mass Spectrom. 2004;15(8):1237–47.
55. Vlasova I, Saletsky A. Raman spectroscopy in investigations of secondary structure of human serum albumin at binding of nanomarkers of fluorescein family. Laser Phys. 2010;20 (9):1844–8.
56. Wen Z, Hecht L, Barron L. alpha-Helix and associated loop signatures in vibrational Raman optical activity spectra of proteins. J Am Chem Soc. 1994;116(2):443–5.
57. Slack SM, Horbett TA. The Vroman effect-A critical review. Proteins Interfaces II. 1995;602:112–28.
58. Roach P, Farrar D, Perry CC. Interpretation of protein adsorption: surface-induced conformational changes. J Am Chem Soc. 2005;127(22):8168–73.
59. Tiselius A, Hjerten S, Levin Ö. Protein chromatography on calcium phosphate columns. Arch Biochem Biophys. 1956;65 (1):132–55.

60. Bernardi G, Giro M-G, Gaillard C. Chromatography of polypeptides and proteins on hydroxyapatite columns: some new developments. Biochim Biophys Acta (BBA)-Protein Struct. 1972;278 (3):409–20.
61. Gorbunoff MJ, Timasheff SN. The interaction of proteins with hydroxyapatite: III. Mechanism. Anal Biochem. 1984;136 (2):440–5.
62. Luo Q, Andrade JD. Cooperative adsorption of proteins onto hydroxyapatite. J Colloid Interface Sci. 1998;200(1):104–13.
63. Garcia AJ, Ducheyne P, Boettiger D. Effect of surface reaction stage on fibronectin-mediated adhesion of osteoblast-like cells to bioactive glass. J Biomed Mater Res. 1998;40(1):48–56.
64. Moawad H, Jain H, editors. Fabrication of nano–macro porous soda-lime phosphosilicate bioactive glass by the melt-quench method. Ceramic engineering and science proceeding; 2007.